Received: 7 December 2024 | Revised: 27 January 2025 | Accepted: 24 April 2025

DOI: 10.1111/php.14115

RESEARCH ARTICLE

Virus inactivation and skin safety studies using far-UVC LEDs

David Welch[1] | **Manuela Buonanno**[1] | **Camryn Petersen**[1] | **Igor Shuryak**[1] | **Thomas Filler**[2] | **Neysha Lobo-Ploch**[2] | **David J. Brenner**[1]

[1]Center for Radiological Research, Columbia University Irving Medical Center, New York, New York, USA

[2]Ferdinand-Braun-Institut (FBH), Berlin, Germany

Correspondence
David Welch, Center for Radiological Research, Columbia University Irving Medical Center, New York, NY, USA.
Email: dw2600@cumc.columbia.edu

Funding information
Open Philanthropy Foundation; Stephen M. Ross Foundation; Flu Lab; Empire State Biodefense Commercialization Fund; National Institute for Occupational Safety and Health, Grant/Award Number: R01OH012312; Columbia University Urban Tech Award; German Federal Ministry of 377 Education and Research (Bundesministerium fur Bildung und Forschung), Grant/Award Number: 03COV10D and 03COV10E

Abstract

Reducing airborne disease transmission is a public health goal. Far-UVC light, defined as 200–235 nm, is a promising technology to inactivate viruses within occupied spaces. This work examines state of the art far-UVC emitting LEDs, with a center emission wavelength of 233 nm, for virus inactivation efficacy and for DNA damage to skin models. The LEDs were used to expose an aerosolized surrogate of SARS-CoV2, the human coronavirus OC43, and survival results estimated a susceptibility constant of $k_{233\text{-aerosol}} = 4.0 \pm 0.2\,cm^2/mJ$, which corresponds to a D_{90} of $0.58\,mJ/cm^2$. HCoV-OC43 was also exposed after drying on a plastic or glass surface, and inactivation results estimated susceptibility values of $k_{1\_233\text{-plastic}} = 6.7 \pm 3.8\,cm^2/mJ$ and $k_{1\_233\text{-glass}} = 7.2 \pm 3.0\,cm^2/mJ$ which were not significantly different. For safety evaluation, human skin biopsies exposed to $100\,mJ/cm^2$ from the 233 nm LEDs indicated only 8% of the epidermal cells were positive for DNA damage, whereas the same dose from a 254 nm lamp showed damage in 45% of epidermal cells. A radiant exposure of $100\,mJ/cm^2$ from the 233 nm LEDs did not produce DNA double strand breaks within the skin biopsies. These tests for the safety and efficacy of a 233 nm far-UVC LED system provide support for the continued development of far-UVC LED sources.

KEYWORDS
far-UVC, LEDs, ultraviolet, virus inactivation

INTRODUCTION

Preventing infectious disease transmission remains a major public health goal. The SARS-CoV-2 pandemic, which is understood to spread through airborne transmission,[1] highlighted the need for novel intervention technologies. Although the immediate threat of SARS-CoV-2 has diminished from its peak, diseases such as SARS-CoV-2, seasonal

Abbreviations: ACGIH, American Conference of Gernmnetal and Industrial Hygienists; CPE, cytopathic effects; DAPI, 4',6-diamidino-2-phenylindole; dH2O, distilled water; DNA, deoxyribonucleic acid; FBS, fetal bovine serum; H&E, hematoxylin and eosin; HPSS++, Hank's balanced salt solution with calcium and magnesium; LEDs, light-emitting diodes; MEM, minimum essential medium; PBS, phosphate buffered saline; PTFE, polytetrafluoroethylene; SARS-Cov2, Severe acute respiratory syndrome coronavirus 2; TCID50, tissue culture infectious dose 50; TLV, Threshold Limit Values; UVC, ultraviolet C; γH2AX, phospho-histone H2A.X (Ser 139).

influenza, and tuberculosis continue to be a major cause of morbidity and mortality across the world.[2] Concerns about airborne disease transmission are also heightened for zoonotic viruses since outbreaks such as avian influenza can disrupt food supply chains, and if left unchecked, these viruses could mutate and become a threat to infect humans.[3] It is also apparent that quickly responding to future pandemics using immunizations is not possible since even the most quickly developed vaccines still require months to produce and distribute on a large scale.[4]

A promising intervention technology to prevent the spread of airborne diseases is exposure of the indoor air to far-UVC ultraviolet radiation, which is defined as a range of ultraviolet wavelengths from 200 to 235 nm.[5,6] There is now significant evidence for both the antimicrobial efficacy and the safety of far-UVC wavelengths. The antimicrobial efficacy of UVC has been established for over 100 years,[7] and recent work has demonstrated far-UVC can effectively inactivate microbes in aerosols, liquids, or on surfaces.[8–19] The aerosol inactivation of viruses with far-UVC is particularly promising, with studies showing aerosolized virus inactivation in small chamber experiments,[11,17,18] room-sized chamber experiments,[12] and in real-world situations.[10] Numerous safety studies on far-UVC wavelengths have been performed to explore possible health hazards from direct exposure to far-UVC radiation.[6] The basis for the safe exposure of humans to far-UVC stems from the absorption of these wavelengths in the outermost layer of cells in the skin or the eye, which prevents damage to the deeper layers of tissue that are associated with adverse health effects. The substantial evidence for the safety of far-UVC wavelengths published in the past few years led to the American Conference of Governmental and Industrial Hygienists (ACGIH) altering their recommended 8-h exposure limits, known as threshold limit values (TVLs), in 2022.[20] The new limits established separate limits for eyes and skin exposures and increased the TLVs for wavelengths less than 240 nm. Even with the altered guidelines, there is still a need for additional research into the possible health hazards from these exposures, especially at wavelengths where gas lamp sources are not available.

The ultraviolet radiation source most widely used in far-UVC research has been the KrCl excimer lamp. While the primary emission of the KrCl lamp is at 222 nm, the lamps also produce longer wavelength UVC up to about 260 nm, and the importance of filtering these longer wavelength contributions has been demonstrated in skin models,[21] animal models,[22] and in humans.[23,24] The KrCl spectrum also contains emissions down to almost 190 nm, and while these are minimal, the filtering of these wavelengths is also important to limit ozone generation.[25–28] Filtered KrCl lamps are relatively power efficient, typically 6–8%,[29] and thin film interference filters have provided narrow bandpass filters with high transmission at 222 nm, but the total cost of far-UVC fixtures (inclusive of lamp, filter, and driver) remains high.

Advancements in the production of visible wavelength light-emitting diodes (LEDs) have made LEDs inexpensive and highly energy efficient. However, the performance of LEDs emitting in shorter far-UVC wavelengths is significantly limited, with power conversion efficiencies below 1%.[30] This study uses a LED system manufactured by the Ferdinand-Braun-Institut, which emits far-UVC radiation with sufficient intensity over a large area, for example, an average irradiance of 21 $\mu W/cm^2$ over the 26 cm × 25.6 cm window of the aerosol exposure chamber used in this study, that makes both safety and efficacy testing realistic to perform.[31–34] Testing far-UVC LEDs such as these provides support for continuing technology development in this area.

MATERIALS AND METHODS

UV sources and measurement

A far-UVC emitting LED system was manufactured by the Ferdinand-Braun-Institut (Berlin, Germany) as previously described.[34] The LEDs emit UV radiation through an incorporated optical filter, manufactured by Technische Universität Berlin (Berlin, Germany), to reduce longer wavelength UVC contributions. The spectral irradiance of the filtered LEDs, previously reported by Glaab et al.,[34] was measured at 20 cm using a BTS2048-UV spectroradiometer (Gigahertz-Optik, Inc., Amesbury, MA) and is plotted in Figure 1. The measured peak of the filtered spectrum was at 233 nm with a full width at half maximum of 7.4 nm.

A KrCl excimer lamp (High Current Electronics Institute, Tomsk, Russia) which emits principally at 222 nm was also utilized in this study. The KrCl lamp was used with the addition of a custom optical filter (Ushio America, Cypress, CA) to reduce the emissions outside the 222 nm peak. Experiments also used a low-pressure mercury lamp emitting primarily at 254 nm (8W, UVLMS-38, Analytik Jena US, Upland, CA).

Irradiance was measured using a calibrated Hamamatsu UV Power Meter (C9536/H9535-222, Hamamatsu Photonics K.K., Japan). Dosimetry for the aerosol exposure experiments was performed with Orthochromic OC-1 film (Orthochrome Inc., Hillsborough, NJ). OC-1 film is marketed as a tool for radiation therapy measurements of ionizing radiation; though its utility in UVC dosimetry has been demonstrated previously.[35–37] The film exhibits a color change upon exposure. The color change is related to radiant exposure using a calibration curve.

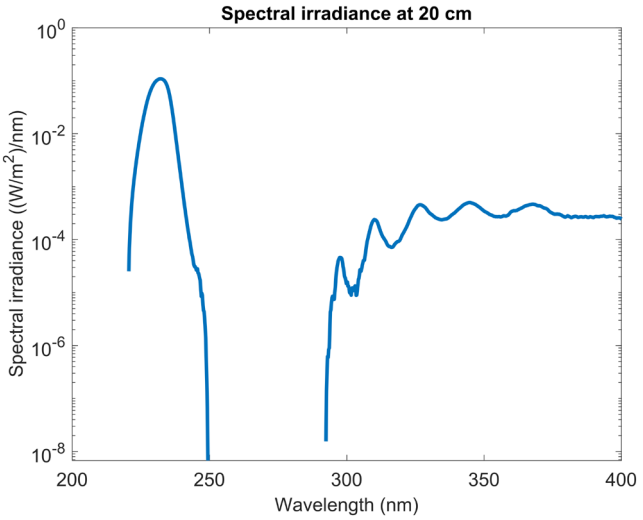

FIGURE 1 The spectral irradiance of the far-UVC emitting LED system manufactured by the Ferdinand-Braun-Institut was measured at 20 cm. The tested LED system includes an optical filter to reduce longer wavelength UVC. The peak emission is at 233 nm with a full-width at half maximum of 7.4 nm.

Viral strain

Human beta-coronavirus OC43 (HCoV-OC43; VR-1558) was propagated in human diploid lung fibroblasts (WI-38; CCL-75) (ATCC, Manassas, VA). The human cell line was grown in MEM supplemented with 10% fetal bovine serum (FBS), 2 mM L-alanyl-L-glutamine, 100 U/mL penicillin, and 100 µg/mL streptomycin (Sigma-Aldrich Corp. St. Louis, MO, USA). The virus infection medium consisted of RPMI-1640 plus 2% heat-inactivated FBS. The viral strain was propagated by inoculation of flasks containing host cells, which were plated the day before at 80–90% confluence. After 2-h incubation, the cell monolayer was washed and incubated in fresh infection medium for 3 or 4 days at 33°C. The supernatant containing the working viral stock was then collected by centrifugation (300 g for 15 min). The virus titer was determined by 50% tissue culture infective dose TCID50 by assessing cytopathic effects (CPE), which were scored at a bright field microscope (10x) as vacuolization of cytoplasm, cell rounding, and sloughing. TCID50 was calculated using standard methodology.[38]

Benchtop aerosol irradiation chamber

The single-pass aerosol exposure chamber used in this study was previously described in detail[11,17,18]; however, a few modifications were made to the exposure setup for testing using the LED system. The exposure system consists of a Blaustein Atomizing Module (CH Technologies, Westwood, NJ) operating in the recirculating configuration for aerosol generation, an exposure volume measuring 26 cm × 25.6 cm × 6.5 cm through which the aerosol passed, a gelatin filter (37 mm, 225–9552, SKC Inc., Eighty Four, PA) for collection of the aerosol following exposure, and the flow through the single-pass system is controlled with a precision flow orifice and a vacuum pump. The system was operated with choked flow conditions across the orifice, which maintained a flow rate of 11.6 LPM using orifice B-47-SS (O'Keefe Controls Co., Monroe, CT) and a flow rate of 5.72 LPM when using orifice B-33-SS (O'Keefe Controls Co.). UV from the LED system entered the chamber through one of the 26 cm × 25.6 cm sides of the exposure volume through a 6 mm thick quartz plate which transmitted 72% of incident UV from the LED system. The opposite 26 cm × 25.6 cm side of the exposure volume was aluminum with a specular mirror finish (Anolux UVS, Anomet Inc., Brampton, ON, Canada) with a reflectance of ~60% for the LED emission wavelengths. The LED system was positioned 20 cm from the quartz window. A 5 µm thick sheet of PTFE (GF63284036, Sigma-Aldrich, Inc., St. Louis, MO) was affixed to the output side of the optical filter on the LED system to diffuse the LED emission pattern and more evenly irradiate across the quartz window area. OC-1 film was used to measure an average irradiance of 21 µW/cm^2 across the quartz window. When accounting for the quartz transmission and the reflectance of the aluminum, the average fluence rate in the exposure volume was estimated at 24 µW/cm^2. The fluence rate was multiplied by the time for a particle to traverse the exposure volume for each flow rate, either 23 or 46.8 s for flow rates of 11.6 LPM or 5.72 LPM, respectively, to calculate the exposure dose for an experiment. The exposure dose could also be reduced for a given flow rate by dimming the LED output using the LED control software. As in our previous studies, the average temperature during testing was 24°C, the relative humidity was between 60 and 70%, and the aerosol size distribution was typical of human coughing, breathing, and talking,[39] with over 90% of particles less than 1.0 µm diameter.

The aerosol for each experiment was generated using a viral solution consisting of 1 mL MEM (Life Technologies, Grand Island, NY) containing 10^7–10^8 TCID50 of virus, 20 mL of deionized water, and 0.05 mL of Hank's balanced salt solution with calcium and magnesium (HBSS^{++}). Each period of aerosol exposure and collection onto a filter lasted 30 min. After the sampling period was completed, the 37-mm gelatin filter which captured the aerosolized virus was dissolved in 5 mL of prewarmed (~32°C) PBS on an orbital shaker for 5 min. The solution was then used for the virus infectivity assays.

Virus exposed on surfaces

A stock of the virus typically containing 10^6–10^7 TCID50 was diluted 1:100 in phosphate buffer saline (PBS). Ten 10-μL drops of the diluted viral solution were pipetted on a 30-mm Petri dish or on 60-mm borosilicate glass Petri dishes (Corning Pyrex). The drops were dried on the surface by leaving the dish uncovered in a laminar flow hood for 30–40 min and then exposed. Immediately after exposure, the virus was collected from the surface by washing with 100 μL of autoclaved dH_2O and assayed for viral infectivity.

Virus infectivity

We used the TCID50 assay to determine viral infectivity. Briefly, ~10^4 host cells were plated in each well of 96-well plates the day prior to the experiment. Cells were washed once in PBS and at least six serial 1:10 dilutions (8 wells for each dilution) in infection medium of the exposed virus were overlaid on host cells for 2 h. The medium was then replaced with fresh infection medium and incubated for 3 or 4 days at 34°C after which CPE was scored and TCID50 calculated.

DNA photodamage analysis in skin models

Live human skin biopsies of in vivo normal human skin (NativeSkin®, Genoskin), which consist of all cell types and skin appendages, were used to analyze DNA damage. The ex vivo biopsies maintain the same histological features of in vivo human skin as well as barrier function, a mature stratum corneum, and a functional basal layer.[40] Through Genoskin, the samples were obtained with the Informed Consent of patients undergoing plastic surgery and in compliance with the Declaration of Helsinki. For each sample, the company provided age, self-identified sex, and phototype that was assigned by a laboratory associate and validated by the biobanking manager based on the Fitzpatrick scale.[41] Samples from two donors were used in this study. The first donor was a 50-year-old female with Fitzpatrick skin type 4. The second donor was a 66-year-old female with Fitzpatrick skin type 4. Biopsies were from the abdomen of the donors.

This study also used the 3-D human skin model EpiDerm-FT (MatTek Corp., Ashland, MA) which is derived from single adult donors. EpiDerm-FT is a full-skin thickness construct that recapitulates the key components of human skin, consisting of 8–12 cell layers of normal human epidermal keratinocytes and dermal fibroblasts that form basal, spinous, granular, and cornified layers analogous to those found in vivo.[42]

Tissues were exposed to a radiant exposure of 100 mJ/cm^2 using either the 233 nm LEDs, the 222 nm lamp, or the 254 nm lamp. After exposure, the tissues were incubated at 37°C for 30 min or 24 h, then fixed overnight in 10% formalin. Induced DNA damage was assessed by standard immunohistochemistry methods using anti-cyclobutane pyrimidine dimers antibody (Cosmo Bio NMDND001, 1:800) or anti-γH2AX antibody (Novus Biologicals NB100-78356, 1:500). Stratum corneum thickness was measured for each Genoskin sample using bright field images of hematoxylin and eosin (H&E) stained skin tissues (5 um) taken at an Olympus IX70 Inverted Phase Contrast DIC Fluorescence Microscope equipped with a Photometrics CoolSNAP HQ2 camera (Teledyne Technologies, Thousand Oaks, CA) and the Image Pro software. For each sample, measurements of the thickness of the stratum corneum were taken over 10 different fields of view (40x) using the distance function of the Image Pro software. The objective was calibrated using a micrometer in Image Pro Plus 6.0 software (Media Cybernetics, Inc., Rockville, Maryland).

Statistical analyses

Inactivation of virus relative to zero-fluence controls was expressed as logs of cell kill [−log10(surviving fraction)] or surviving fraction, following exposure on surfaces or aerosol to different radiant exposures. The fractional inactivation as a function of the UV radiant exposure is expressed as $TCID50_{UV}/TCID50_{controls}$ for viruses. All dose–responses were modeled to follow a single-phase exponential decay using $S = e^{-kD}$, where S is the surviving fraction, k (cm^2/mJ) is the inactivation rate constant, and D is the dose in mJ/cm^2. Linear regression was performed using normalized ln[S] values as the dependent variable and UV dose (D, mJ/cm^2) as the independent variable. The linear regression was performed with the intercept term set to zero, representing the definition of 100% relative survival at zero UV dose.

Results for the surface inactivation tests were also fit to a bi-exponential decay model commonly used in disinfection and pathogen inactivation analyses.[43] This model describes a bi-exponential dose–response, where one exponential describes the behavior of a susceptible fraction of the population, and the second exponential describes the response of a more resistant subpopulation:

$$S = (1 - f)\, e^{-k_1 D} + f e^{-k_2 D} \quad (1)$$

where S is the non-inactivated (surviving) fraction of the microbe and D is the radiant exposure dose in mJ/cm^2. $(1-f)$ and f are respectively the proportions of the sensitive and the resistant subpopulations whose exponential dose responses are defined by parameters k_1 and k_2 (units of cm^2/mJ). The performance of the single- and bi-exponential models was compared using the Akaike information criterion (AIC)[44] to verify which model provided a better fit. Results for the surface inactivation study were also analyzed using a linear-quadratic polynomial function regression to the dependence of −ln(S) as a function of dose, for glass and plastic separately. Random effects by experiment were included to account for systematic differences between the two experimental batches within each material.[45]

The inactivation cross-section D_{90} (i.e., the UV dose that inactivates 90% of the exposed virus) was calculated as $D_{90} = -\ln(1-0.90)/k$. Only the k_1 value was used to calculate D_{90} for the results fit to the biexponential model. Unpaired t-tests were performed to compare averages, and a value of $p < 0.05$ was considered statistically significant.

DNA damage yields represent the average ± standard error of the mean (SEM) of keratinocytes exhibiting dimers or gH2AX foci measured in at least six randomly selected fields of view for each sample ($n = 2$). For both markers, between 600 and 2100 cells were counted. Comparisons of mean values between treatment groups and controls were performed using Student's t-test.

RESULTS

Efficacy of 233 nm LED to inactivate airborne virus

Results for the inactivation of aerosolized HCoV OC43 using the 233 nm LED system are plotted in Figure 2. Using the single-phase exponential decay model, the inactivation rate constant for the 233 nm LEDs was $k_{233\text{-aerosol}} = 4.0 \pm 0.2\,\text{cm}^2/\text{mJ}$, which corresponds to a D90 (i.e., the UV dose that inactivates 90% of the exposed virus) of 0.58 mJ/cm^2.

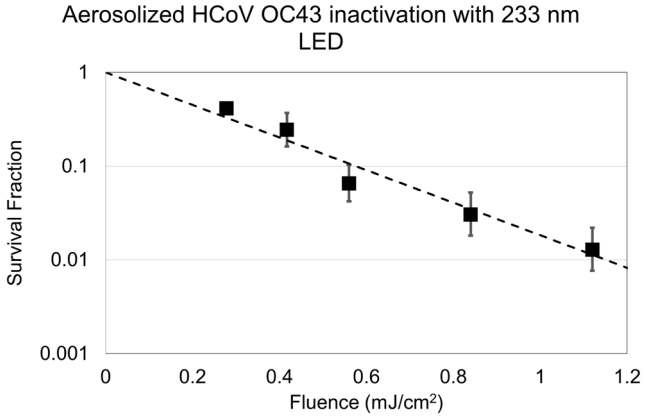

FIGURE 2 Inactivation of aerosolized human OC43 coronavirus exposed to the UV radiation from LEDs with a peak wavelength of 233 nm in a benchtop aerosol chamber. Fractional survival of the virus was analyzed using the TCID50 assay. Values are reported as mean ± SD. The single-phase exponential decay model with $k_{233\text{-aerosol}} = 4.0 \pm 0.2\,\text{cm}^2/\text{mJ}$ is also plotted.

Exposure surface material does not affect HCoV OC43 susceptibility

Surface efficacy studies are typically conducted using polypropylene Petri dishes. However, it has been shown that exposure of plastics itself to UV light in the presence of oxygen may lead to the formation of cytotoxic free radicals.[46–48] To determine whether the surface material influenced the susceptibility of microorganisms to far-UVC, we compared the dose–response of human coronavirus OC43 when exposed on plastic (polypropylene) or (borosilicate) glass dishes. Results for the inactivation of HCoV OC43 on either plastic or glass are plotted in Figure 3. The results for each surface were fit to single- and bi-exponential decay models, and in each case, the AIC score difference favored the bi-exponential model. Using the bi-exponential model, the inactivation rate constants when exposed on plastic were $k_{1\_233\text{-plastic}} = 6.7 \pm 3.8\,\text{cm}^2/\text{mJ}$ and $k_{2\_233\text{-plastic}} = 0.97 \pm 1.1\,\text{cm}^2/\text{mJ}$, with the resistant subpopulation estimated to be $f_{233\text{-plastic}} = 0.07$. For the glass surface, the inactivation rate constants were $k_{1\_233\text{-glass}} = 7.2 \pm 3.0\,\text{cm}^2/\text{mJ}$ and $k_{2\_233\text{-glass}} = 0.27 \pm 1.1\,\text{cm}^2/\text{mJ}$ with the resistant subpopulation estimated to be $f_{233\text{-glass}} = 0.02$. The D_{90} (i.e., the UV dose that inactivates 90% of the exposed virus) for plastic was estimated to be 0.34 mJ/cm^2. For a glass surface, the D_{90} was estimated to be 0.32 mJ/cm^2. When evaluating data with a random effects model to account for systematic differences between the experiments, there was no significant difference found between the susceptibility of the HCoV OC43 on plastic and glass ($p > 0.05$).

DNA damage in exposed skin tissue samples

Genoskin human skin biopsy samples were analyzed for CPD formation within the epidermis. Multiple randomly selected fields of view were analyzed across the skin tissues to determine the average number of CPD positive cells over the entire epidermis. CPD yields represent the average ± standard deviation (SD) of keratinocytes exhibiting dimers divided by the total number of cells measured. The

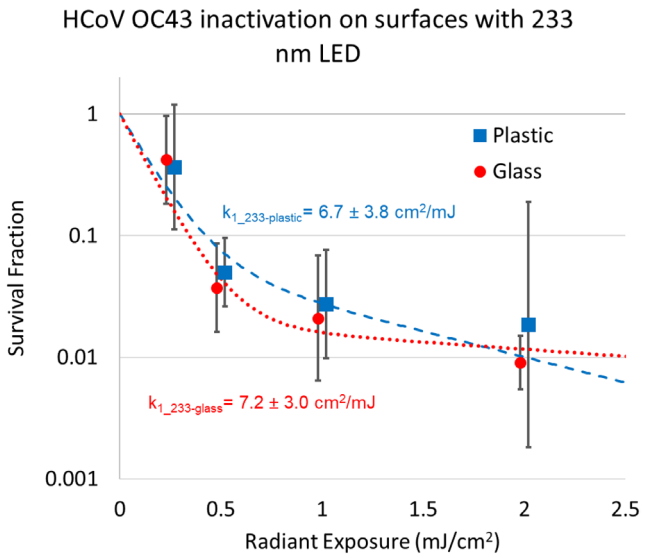

FIGURE 3 Inactivation of dried HCoV OC43 exposed on either a plastic or glass surface to UV radiation from LEDs with a peak wavelength of 233 nm. Fractional survival of the virus was analyzed using the TCID50 assay. Values are reported as mean ± SD. Datapoints of the same radiant exposure are slightly offset so error bars are visible. Bi-exponential decay models for each of the materials are also included on the plot.

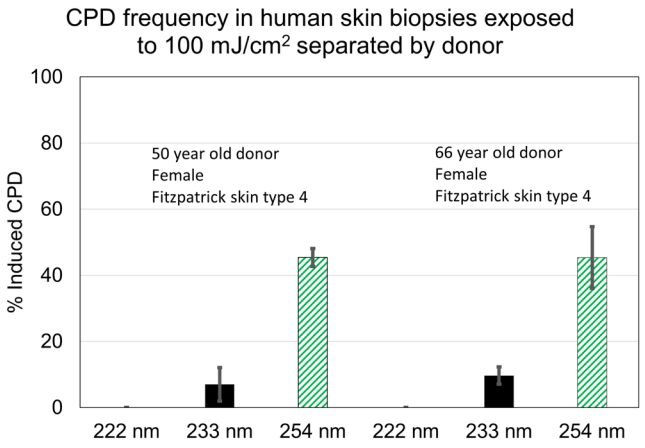

FIGURE 4 The CPD frequency within the epidermal layer after exposure to 100 mJ/cm^2 from different UVC sources is plotted for biopsies from two donors. Values are reported as mean ± SD.

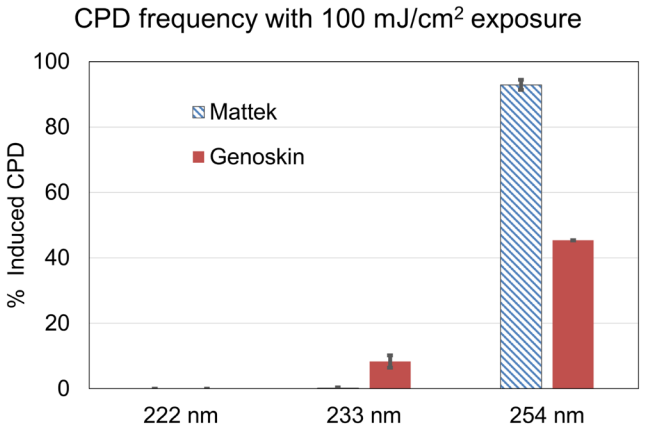

FIGURE 5 CPD frequency within the epidermal layer is plotted for two skin models. A radiant exposure of 100 mJ/cm^2 was used for the tested UV sources at 222 nm, 254 nm, or 233 nm. Tissues were fixed 30 min after exposure. Values are reported as mean ± SD.

total number of cells was determined by counting the number of nuclei positive for 4′,6-diamidino-2-phenylindole (DAPI) using the coverslip mounting medium with DAPI (Vectashield, Burlingame, CA). Results for CPD frequency in samples fixed 30 min after exposure are plotted in Figure 4. Data are shown for each donor separately. The stratum corneum thickness for the tissue from the 50-year-old donor was 10.1 ± 1.2 µm, and the thickness for tissue from the 66 year-old donor was 10.2 ± 1.6 µm.

The exposed Genoskin tissues were also analyzed for the induction of phospho-histone H2A.X (Ser 139) foci also known as γH2AX foci, which are typically associated with DNA double strand breaks induced by ionizing radiation.[49] A radiant exposure of 100 mJ/cm^2 from the 254 nm lamp yielded 4.3 ± 0.9% positive keratinocytes within the epidermis, while exposures with the 222 nm lamp and the 233 nm LED did not produce γH2AX-positive cells.

Mattek EpiDerm-FT skin models were analyzed for CPD frequency within the epidermis. Results are shown in Figure 5 separated by exposure wavelength. Also included in Figure 5 are the results from the Genoskin tissues using combined data from the two donors.

DISCUSSION

The idea of using far-UVC technology to help prevent the spread of disease within occupied environments continues to gain popularity; however, this approach is still limited by the relatively high cost of optically filtered KrCl lamp fixtures, which are the only viable far-UVC sources for room-scale exposures currently available. Newly developed far-UVC sources such as the 233 nm LEDs tested in this work offer promise that LEDs with the emission wavelengths and power output necessary for effectively inactivating viruses in the air and on surfaces can be produced. The results of this study, which to the best of our knowledge include the first analysis on the airborne inactivation of a virus using a far-UVC LED source, provide data to support further improvements in far-UVC LED manufacturing processes to enable larger room-scale efficacy testing and eventually the installation of far-UVC LEDs in a real-world setting to prevent disease transmission.

Estimation of inactivation rates of aerosolized viruses using a far-UVC source is particularly important for the

design and analysis of far-UVC systems. In this study using a single-pass benchtop exposure chamber and the 233 nm LED system, the susceptibility of HCoV OC43 was $k_{233\text{-aerosol}} = 4.0 \pm 0.2\,cm^2/mJ$, which suggests these LEDs are slightly less effective than a filtered KrCl lamp at 222 nm, which produced an estimated susceptibility of $k = 12.4\,cm^2/mJ$ under similar experimental conditions.[17] While the timeline and success of far-UVC LED development are uncertain, the prospect of LEDs being lower cost, more energy efficient, and with more freedom in module design than a gas lamp could eventually make LEDs a more attractive far-UVC source than current KrCl lamps, which would offset any potential difference in inactivation efficacy. Furthermore, the longer wavelength 233 nm LEDs could potentially be more effective than 222 nm lamps when the suspending media includes mucin or other components that may attenuate the UV within the aerosol.[15] Questions remain regarding the translation of benchtop chamber results to real-world results since tests in both a room-sized chamber[12] and within a real-world installation[10] have implied virus susceptibility values that are significantly higher than values determined in a small laboratory chamber. Overall, it is apparent that further studies examining the susceptibility of aerosolized viruses to far-UVC exposure both in a laboratory setting and within real-world installations are needed to more fully understand the antimicrobial efficacy.

The inactivation tests of HCoV OC43 dried on a plastic or glass surface and exposed using the 233 nm LEDs estimated a susceptibility of $k_{1\_233\text{-plastic}} = 6.7 \pm 3.8\,cm^2/mJ$ or $k_{1\_233\text{-glass}} = 7.2 \pm 3.0\,cm^2/mJ$. Previous studies have tested the inactivation of coronaviruses suspended in water. For example, results from Boegel et al. used 254 nm irradiation and reported a k-value of ~1.3 cm^2/mJ for SARS-CoV-2, HCoV 229E, and HCoV OC43.[50] Ma et al. examined HCoV 229E inactivation in water using various UV sources, and their results estimated $k = 0.84\,cm^2/mJ$ for a filtered 222 nm KrCl lamp and $k = 0.59\,cm^2/mJ$ for a 254 nm lamp.[14] The higher susceptibility observed using LEDs in this study could be attributed to the virus being dried on the surface during exposure, which typically results in higher susceptibility than when exposed in liquid.[43]

This study examined the possibility of a plastic or glass surface influencing the susceptibility of a virus. Previous research suggested that exposure of plastic to UVC or UVB in the presence of oxygen may cause photooxidation,[46–48] leading to the formation of free radicals which would interact with viruses present on the surface. Other studies explored the possibility that UV exposure of polypropylene generates cytotoxic hydroperoxides and carboxylic acids[51,52] that could enhance the inactivation of the plated living organisms they are in contact with. The results in this study compared the dose–response of human coronavirus OC43 using a 233 nm LED source when exposed on plastic (polypropylene) or (borosilicate) glass dishes (Figure 3) and no difference in virus susceptibility on the two materials was observed. The doses used in these surface inactivation studies, with a maximum of only 2 mJ/cm^2, are orders of magnitude less than the doses in the studies reported to cause plastic photooxidation or other photochemistry products, so the magnitude of these products is likely also much less; regardless, the results in this work do not suggest such products are influencing virus susceptibility by using plastic substrates instead of less reactive glass surfaces.

Important to the use of far-UVC is the potential for safe exposure of occupants while performing air and surface inactivation. This study used two types of human skin models to examine the induction of photodamage as an indication of relative safety. The Genoskin tissues were biopsied from human donors and therefore represent a complete skin model. Tissues from the two donors responded similarly for all exposure wavelengths. Thirty minutes after exposure, no CPDs were observed in the 222 nm exposed samples, while ~8% of the epidermal cells were positive for CPDs when exposed to 100 mJ/cm^2 using the 233 nm LEDs, and ~45% of the epidermal cells were positive for CPDs when exposed to 100 mJ/cm^2 using a 254 nm lamp. Although CPDs were present in these tissues immediately after exposure, the repair of the CPDs or the progression of the keratinocytes into corneocytes and eventually sloughing off is not evident at this timepoint. Future work with these or similar far-UVC LEDs could benefit from using animal or human exposures and additional endpoints to evaluate the threshold dose more fully for acute effects from these LEDs. It is also worthwhile to note that these donors were both Fitzpatrick skin type 4, so photodamage could be higher in individuals with lighter skin. Extending analysis to include a range of skin types and ages could provide insight into how these factors impact safety considerations.

The analysis of γH2AX foci formation, a marker of DNA double strand breaks in the exposed Genoskin tissue only showed such damage from the 254 nm exposure. While γH2AX is not a typical marker used for photodamage, this endpoint is useful to show the relative safety of both the far-UVC exposures at both 233 and 222 nm.

Using the Mattek EpiDerm-FT in vitro skin model to examine photodamage is useful since the model is uniform and reproducible between experiments. Our previous work with a monochromatic source exposing Mattek EpiDerm-FT tissue showed a dramatic change in CPD induction across the UVC range.[53] The results from this study again show this effect, with a 100 mJ/cm^2 254 nm exposure inducing CPDs in 93% of the epidermal cells and essentially no CPDs when using either the 222 or 233 nm far-UVC sources. The minimal amount of CPDs following

the 233 nm LED exposure agrees with our previous results using a monochromatic source at 230 or 235 nm, with CPD showing only in the uppermost layer of the epidermis,[53] and with results obtained in other laboratories.[33,34] Generally, the Genoskin tissue could be expected to have fewer CPDs than the Mattek EpiDerm-FT for the same exposure since melanin or other materials that absorb in the far-UVC are not present in the Mattek EpiDerm-FT model; however, the results at 233 nm showed more CPDs in the Genoskin model. This result could be attributed to the non-uniform structure of the Genoskin, which can yield variations in the stratum corneum thickness across the exposure area that are not present in the in vitro Mattek EpiDerm-FT model.

These tests for the safety and efficacy of a 233 nm far-UVC LED system provide support for the continued development of far-UVC LED sources. Further advancements in LED technology will enable more options for testing efficacy and safety at a larger scale, and could eventually lead to room-scale installations to decrease disease transmission and improve public health.

ACKNOWLEDGMENTS

This work was supported by the Open Philanthropy Foundation, the Stephen M. Ross Foundation, Flu Lab, the Empire State Biodefense Commercialization Fund, CDC NIOSH Grant R01OH012312, a Columbia University Urban Tech Award, and the German Federal Ministry of 377 Education and Research (Bundesministerium fur Bildung und Forschung) under contracts 03COV10D and 03COV10E.

DATA AVAILABILITY STATEMENT

The data that support the findings of this study are available from the corresponding author upon reasonable request.

ORCID

David Welch https://orcid.org/0000-0003-2784-496X

REFERENCES

1. Greenhalgh T, Jimenez JL, Prather KA, Tufekci Z, Fisman D, Schooley R. Ten scientific reasons in support of airborne transmission of SARS-CoV-2. *Lancet*. 2021;397(10285):1603-1605.
2. Nardell EA. Indoor environmental control of tuberculosis and other airborne infections. *Indoor Air*. 2016;26(1):79-87.
3. Wille M, Barr IG. Resurgence of avian influenza virus. *Science*. 2022;376(6592):459-460.
4. Burgos RM, Badowski ME, Drwiega E, et al. The race to a COVID-19 vaccine: opportunities and challenges in development and distribution. *Drugs in Context*. 2021;10:2020-12-2. doi:10.1007/s40260-021-00865-8
5. Blatchley ER III, Brenner DJ, Claus H, et al. Far UV-C radiation: an emerging tool for pandemic control. *Crit Rev Environ Sci Technol*. 2023;53(6):733-753.
6. Görlitz M, Justen L, Rochette PJ, et al. Assessing the safety of new germicidal far-UVC technologies. *Photochem Photobiol*. 2024;100(3):501-520.
7. Reed NG. The history of ultraviolet germicidal irradiation for air disinfection. *Public Health Rep*. 2010;125(1):15-27.
8. Beck SE, Hull NM, Poepping C, Linden KG. Wavelength-dependent damage to adenoviral proteins across the germicidal UV Spectrum. *Environ Sci Technol*. 2017;52(1):223-229. doi:10.1021/acs.est.7b04602
9. Beck SE, Rodriguez RA, Linden KG, Hargy TM, Larason TC, Wright HB. Wavelength dependent UV inactivation and DNA damage of adenovirus as measured by cell culture infectivity and long range quantitative PCR. *Environ Sci Technol*. 2014;48(1):591-598.
10. Buonanno M, Kleiman NJ, Welch D, Hashmi R, Shuryak I, Brenner DJ. 222 nm far-UVC light markedly reduces the level of infectious airborne virus in an occupied room. *Sci Rep*. 2024;14(1):6722.
11. Buonanno M, Welch D, Shuryak I, Brenner DJ. Far-UVC light (222 nm) efficiently and safely inactivates airborne human coronaviruses. *Sci Rep*. 2020;10(1):10285.
12. Eadie E, Hiwar W, Fletcher L, et al. Far-UVC (222 nm) efficiently inactivates an airborne pathogen in a room-sized chamber. *Sci Rep*. 2022;12(1):4373.
13. Ma B, Gundy PM, Gerba CP, Sobsey MD, Linden KG. UV inactivation of SARS-CoV-2 across the UVC Spectrum: KrCl* excimer, mercury-vapor, and light-emitting-diode (LED) sources. *Appl Environ Microbiol*. 2021;87(22):e0153221.
14. Ma B, Linden YS, Gundy PM, Gerba CP, Sobsey MD, Linden KG. Inactivation of coronaviruses and phage Phi6 from irradiation across UVC wavelengths. *Environ Sci Technol Lett*. 2021;8(5):425-430.
15. Schuit MA, Larason TC, Krause ML, et al. SARS-CoV-2 inactivation by ultraviolet radiation and visible light is dependent on wavelength and sample matrix. *J Photochem Photobiol B Biol*. 2022;233:112503.
16. Seuylemezian A, Buonanno M, Guan L, Brenner DJ, Welch D. Far-UVC light as a new tool to reduce microbial burden during spacecraft assembly. *Adv Space Res*. 2021;67(1):496-503.
17. Welch D, Buonanno M, Buchan AG, et al. Inactivation rates for airborne human coronavirus by low doses of 222 nm far-UVC radiation. *Viruses*. 2022;14(4):684.
18. Welch D, Buonanno M, Grilj V, et al. Far-UVC light: a new tool to control the spread of airborne-mediated microbial diseases. *Sci Rep*. 2018;8(1):2752.
19. Petersen C, Buonanno M, Guan L, et al. Susceptibility of extremophiles to far-UVC light for bioburden reduction in spacecraft assembly facilities. *Life Sci Space Res*. 2024;41:56-63.
20. American Conference of Governmental Industrial Hygienists. *2022 Threshold Limit Values and Biological Exposure Indices*. American Conference of Governmental Industrial Hygienists; 2022.
21. Buonanno M, Welch D, Brenner DJ. Exposure of human skin models to KrCl excimer lamps: the impact of optical filtering. *Photochem Photobiol*. 2021;97(3):517-523.
22. Narita K, Asano K, Yamane K, Ohashi H, Igarashi T, Nakane A. Effect of ultraviolet C emitted from KrCl excimer lamp with or without bandpass filter to mouse epidermis. *PLoS One*. 2022;17(5):e0267957.

23. Eadie E, Barnard IM, Ibbotson SH, Wood K. Extreme exposure to filtered far-UVC: a case study. *Photochem Photobiol*. 2021;97(3):527-531.
24. Woods JA, Evans A, Forbes PD, et al. The effect of 222-nm UVC phototesting on healthy volunteer skin: a pilot study. *Photodermatol Photoimmunol Photomed*. 2015;31(3):159-166. doi:10.1111/phpp.12156
25. Barber VP, Goss MB, Franco Deloya LJ, et al. Indoor air quality implications of germicidal 222 nm light. *Environ Sci Technol*. 2023;57(42):15990-15998.
26. Claus H. Ozone generation by ultraviolet lamps. *Photochem Photobiol*. 2021;97(3):471-476.
27. Link MF, Shore A, Hamadani BH, Poppendieck D. Ozone generation from a germicidal ultraviolet lamp with peak emission at 222 nm. *Environ Sci Technol Lett*. 2023;10(8):675-679.
28. Peng Z, Day DA, Symonds GA, et al. Significant production of ozone from germicidal UV lights at 222 nm. *Environ Sci Technol Lett*. 2023;10(8):668-674.
29. Pattison M, Hansen M, Bardsley N, et al. *Solid-State Lighting R&D Opportunities*. Guidehouse, Inc.; 2022.
30. Kneissl M, Seong TY, Han J, Amano H. The emergence and prospects of deep-ultraviolet light-emitting diode technologies. *Nat Photonics*. 2019;13(4):233-244.
31. Busch L, Kröger M, Schleusener J, et al. Evaluation of DNA lesions and radicals generated by a 233 nm far-UVC LED in superficial ex vivo skin wounds. *J Photochem Photobiol B Biol*. 2023;245:112757.
32. Lobo-Ploch N, Mehnke F, Sulmoni L, et al. Milliwatt power 233 nm AlGaN-based deep UV-LEDs on sapphire substrates. *Appl Phys Lett*. 2020;117(11):111102.
33. Zwicker P, Schleusener J, Lohan SB, et al. Application of 233 nm far-UVC LEDs for eradication of MRSA and MSSA and risk assessment on skin models. *Sci Rep*. 2022;12(1):2587.
34. Glaab J, Lobo-Ploch N, Cho HK, et al. Skin tolerant inactivation of multiresistant pathogens using far-UVC LEDs. *Sci Rep*. 2021;11(1):14647.
35. Welch D, Brenner DJ. Improved ultraviolet radiation film dosimetry using OrthoChromic OC-1 film. *Photochem Photobiol*. 2021;97(3):498-504.
36. Duncan MA, Welch D, Shuryak I, Brenner DJ. Ocular and facial far-UVC doses from ceiling-mounted 222 nm far-UVC fixtures. *Photochem Photobiol*. 2023;99(1):160-167.
37. Welch D, Hashmi R, Petersen C, Erde S, Brenner DJ, Nardell E. Film dosimetry for occupant exposure monitoring within far-UVC installations. *Photochem Photobiol*. 2024;101(1):157-166. doi:10.1111/php.13960
38. Lindenbach BD. Measuring HCV infectivity produced in cell culture and in vivo. *Methods Mol Biol*. 2009;510:329-336.
39. Papineni RS, Rosenthal FS. The size distribution of droplets in the exhaled breath of healthy human subjects. *J Aerosol Med*. 1997;10(2):105-116.
40. De Wever B, Kurdykowski S, Descargues P. Human skin models for research applications in pharmacology and toxicology: introducing NativeSkin®, the "missing Link" bridging cell culture and/or reconstructed skin models and human clinical testing. *Appl In Vitro Toxicol*. 2015;1(1):26-32.
41. Fitzpatrick TB. Soleil et peau. *J Med Esthet*. 1975;2:33-34.
42. Kubilus J, Hayden PJ, Ayehunie S, et al. Full thickness EpiDerm: a dermal-epidermal skin model to study epithelial-mesenchymal interactions. *Altern Lab Anim*. 2004;32(Suppl 1A):75-82.
43. Kowalski WJ. *Ultraviolet Germicidal Irradiation Handbook: UVGI for Air and Surface Disinfection*. Springer; 2009.
44. Wagenmakers E-J, Farrell S. AIC model selection using Akaike weights. *Psychon Bull Rev*. 2004;11(1):192-196.
45. R Core Team. *R: A Language and Environment for Statistical Computing*. 2021. https://www.R-project.org/
46. Hankett JM, Collin WR, Chen Z. Molecular structural changes of plasticized PVC after UV light exposure. *J Phys Chem B*. 2013;117(50):16336-16344.
47. Hernández CG, González R, Soto JJ, Rosales I. *Photo-Oxidation of Polystyrene Film Irradiated with UV-B*. Springer International Publishing; 2017.
48. Geuskens G, Baeyens-Volant D, Delaunois G, Vinh QL, Piret W, David C. Photo-oxidation of polymers—II: the sensitized decomposition of hydroperoxides as the main path for initiation of the photo-oxidation of polystyrene irradiated at 253.7 nm. *Eur Polym J*. 1978;14(4):299-303.
49. Rogakou EP, Pilch DR, Orr AH, Ivanova VS, Bonner WM. DNA double-stranded breaks induce histone H2AX phosphorylation on serine 139*. *J Biol Chem*. 1998;273(10):5858-5868.
50. Boegel SJ, Gabriel M, Sasges M, et al. Robust evaluation of ultraviolet-C sensitivity for SARS-CoV-2 and surrogate coronaviruses. *Microbiol Spectr*. 2021;9(2):e00537-21. doi:10.1128/Spectrum.00537-21
51. Otocka EP, Curran S, Porter RS. Photooxidation of polystyrene: irradiation at 254 and 365 nm. *J Appl Polym Sci*. 1983;28(10):3228-3233.
52. Onyiriuka EC. The effects of high-energy radiation on the surface chemistry of polystyrene: a mechanistic study. *J Appl Polym Sci*. 1993;47(12):2187-2194.
53. Welch D, Aquino de Muro M, Buonanno M, Brenner DJ. Wavelength-dependent DNA Photodamage in a 3-D human skin model over the far-UVC and germicidal UVC wavelength ranges from 215 to 255 nm. *Photochem Photobiol*. 2022;98:1167-1171.

How to cite this article: Welch D, Buonanno M, Petersen C, et al. Virus inactivation and skin safety studies using far-UVC LEDs. *Photochem Photobiol*. 2026;102:48-56. doi:10.1111/php.14115